Atoms **2014**, *2*, 277-298; doi:10.3390/atoms2020277

OPEN ACCESS

atoms

ISSN 2218-2004

www.mdpi.com/journal/atoms

Article

Spectral Line Shapes of He I Line 3889 Å

Banaz Omar [1,*], Manuel Á. González [2], Marco A. Gigosos [3], Tlekkabul S. Ramazanov [4], Madina C. Jelbuldina [4], Karlygash N. Dzhumagulova [4], Mark C. Zammit [5], Dmitry V. Fursa [5] and Igor Bray [5]

[1] Institute of Physics, University of Rostock, Rostock 18051, Germany

[2] Departamento de Física Aplicada, Universidad de Valladolid, Valladolid 47071, Spain; E-Mail: manuelgd@termo.uva.es

[3] Departamento de Óptica, Universidad de Valladolid, Valladolid 47071, Spain; E-Mail: gigosos@coyanza.opt.cie.uva.es

[4] Scientific Research Institute for Experimental and Theoretical Physics of Al-Farabi Kazakh National University, Almaty, Kazakhstan; E-Mails: ramazan@physics.kz (T.S.R.), zholboldy@mail.ru (M.C.J.), dzhumagulova.karlygash@gmail.com (K.N.D.)

[5] Institute of Theoretical Physics, Curtin University, Perth, WA 6845, Australia; E-Mails: mark.zammit@postgrad.curtin.edu.au (M.C.Z.), d.fursa@curtin.edu.au (D.V.F.), I.Bray@curtin.edu.au (I.B.)

***** Author to whom correspondence should be addressed; E-Mail: b.omar@dr.com; Tel.: +46 722 758100.

Received: 31 March 2014; in revised form: 5 June 2014 / Accepted: 10 June 2014 / Published: 23 June 2014

Abstract: Spectral line shapes of neutral helium 3889 Å (2^3S–3^3P) transition line are calculated by using several theoretical methods. The electronic contribution to the line broadening is calculated from quantum statistical many-particle theory by using thermodynamic Green's function, including dynamic screening of the electron-atom interaction. The ionic contribution is taken into account in a quasistatic approximation, where a static microfield distribution function is presented. Strong electron collisions are consistently considered with an effective two-particle T-matrix approach, where Convergent Close Coupling method gives scattering amplitudes including Debye screening for neutral helium. Then the static profiles converted to dynamic profiles by using the Frequency Fluctuation Model. Furthermore, Molecular Dynamics simulations for interacting and independent particles are used where the dynamic sequence of microfield is taken into account. Plasma parameters are diagnosed and good agreements are shown by comparing our

theoretical results with the recent experimental result of Jovićević *et al.* (*J. Phys. B: At. Mol. Opt. Phys.* 2005, *38*, 1249). Additionally, comparison with various experimental data in a wide range of electron density $n_e \approx (10^{22} - 10^{24})\,\mathrm{m}^{-3}$ and temperature $T \approx (2-6) \times 10^4$ K are presented.

Keywords: spectral line shapes; Green's function; T-matrix; molecular dynamics simulations; microfield distribution function; plasma diagnostics

1. Introduction

Calculation of spectral line shapes is a most powerful tool for plasma diagnostic in both the star atmosphere and in laboratory plasmas. Perturbation of the radiating atom or ion by the surrounding particles leads to spectral line broadening (Stark broadening), while the coherent emission process is interrupted by collisions and influenced by plasma microfield. Several theoretical approaches have been applied to calculate Stark broadening, such as the well known semiclassical approximation the standard theory (ST) by Griem [1], or the quantum statistical approach of many-particle theory [2], where the motion of ion perturber is neglected during the inverse halfwidth of the line. Furthermore, the model microfield method (MMM) [3–6], the frequency fluctuation method (FFM) [7] or computer simulations [8–11] are used for calculating the line broadening including ion-dynamics effects, which lead to further broadening of the line shapes.

In this work, we describe several theoretical approaches to study the He I 3889Å (2^3S–3^3P) transition line. Plasma parameters are determined by comparing our theoretical results with the measurement of Jovićević *et al.* [12]. In our quantum statistical approach, thermodynamic Green's function is used for calculating emitted or absorbed radiation from bound–bound transition of charge particles by using two-particle polarization function [13–16], which is related to the Fourier transformation of the imaginary part of the dipole–dipole correlation function. In principle, this approach is able to describe the dynamic screening and strong collision by electrons in a systematic way. The quantum statistical approach can adequately treat electron collisions. To obtain full profiles, it has been supplemented by a calculation of ion broadening done by other methods and thereby has been successfully applied to calculate the line profile of hydrogen and H-like ions [17]. The strong collisions of an electron-emitter pair are treated within a T-matrix approach by solving close-coupling equations to produce forward scattering amplitudes. Ions are treated in a quasistatic approximation via the microfield distribution function. Then the latest formulation of the FFM is applied to account for ion dynamics [18]. On the other hand, computer simulations accounting simultaneously for the electronic and ionic fields on the same footing are used for comparison. Recently, the shift and width of this line was computed by Lorenzen *et al.* [19], comparison was made with various theoretical and measurement data in a wide range of electron density and temperature. In Section 2 we describe briefly the experimental setup and result of Jovićević *et al.* [12]. Our theoretical approaches for calculating the line shapes are reviewed in Section 3, followed by results and discussions Section 4.

2. Experiment

In this paper, we analyze theoretically the He I 3889 Å Stark broadening, measured by Jovićević *et al.* [12] from a pulsed low-pressure capillary discharge. The plasma was a mixture of neon, helium and hydrogen, with the predominant H^+ perturber ions. Originally the experiment was set up for the measurement of Ne I spectral line profiles, while He was added to the gas mixture for plasma diagnostic purpose. The presence of hydrogen increases the electron density to the required value until a constant value of the Stark width was recorded. The optimum gas mixture was determined in a series of measurements starting from pure neon and then diluting until optically thin Ne I lines were recorded. In the experiment, a quartz discharge tube with 3 mm inner diameter and length of 7.2 cm was used, and aluminum electrodes with 3 mm diameter holes were located 200 mm apart. The measurements were performed in a premixed gas mixture of 2.4% Ne, 5.6% He and 92% H_2 by volume, at an initial pressure of 4 mbar. Spectroscopic plasma observations of Ne I and He I lines were performed, measuring the line shapes at the same time of plasma decay. The dilution of neon and helium with hydrogen was done in order to increase the electron density, since H has much lower ionization potential than Ne and He, and to generate a plasma with H^+ ions dominating He^+ and Ne^+. Special care was taken to keep the line profiles optically thin during measurements, in order to minimize self-absorption. This was achieved by using a continuous gas flow and diluting neon with helium and hydrogen in the operated arc. Moreover, plasma radiation was observed from the axial narrow discharge tube as well as from the radial expanded part simultaneously. However, the experimental design and procedure may have resulted in plasma inhomogeneity which may cause line distortion and line asymmetry. Electron density was determined from the measured He I line profiles, which were assumed to be optically thin under the same plasma conditions. The experimental profiles were fitted to a semiclassical calculation using two parameters, the electron impact width and the ion-broadening parameter A of the quasistatic approximation [1], which allow the authors to determine the electron density. The mean value of electron density n_e was estimated to be $4.8 \times 10^{22}\ \mathrm{m}^{-3}$ with an estimated uncertainty of $\pm 10\%$. By assuming local thermal equilibrium, the electron temperature $T_e = T_i = 3.3 \times 10^4$ K was determined from the Boltzmann plot of O II impurity lines with an uncertainty of $\pm 12\%$, as the Stark broadening parameters weakly depend upon T_e. More details about the experimental set up and measurement are given in [12].

3. Theoretical Approaches

In this section we present the different kinds of theoretical approaches that we used for calculating He I line profiles.

3.1. Quantum Statistical Approach

In quantum statistical many-particle theory, the medium effects are taken into account by using the thermodynamic Green's function technique to describe the Stark broadening. The perturbing electrons and ions can be treated independently due to variety of mass between them ($m_e << m_i$). The dynamically screened Born approximation applied for electron-emitter interaction, while almost stationary heavy ions are treated in a quasistatic ion approximation

due to static microfield. Spectral line broadening is given by the imaginary part of the second order two-particle polarization function, which is a bound–bound transition. The polarization function is calculated in a systematic way from thermodynamic Green's functions and is proportional to the Fourier transform of the dipole–dipole autocorrelation function (see Appendix A). The perturber–radiator interaction leads to the pressure broadening, including both the electronic and the ionic contributions in the quasistatic limit by averaging the static microfield distribution function $W(\beta)$ [14–16], and we get

$$I^{\rm pr}(\omega) \sim \sum_{i',i'',f',f''} \langle i'|\mathbf{r}|f'\rangle\langle f''|\mathbf{r}|i''\rangle \frac{\omega^4}{8\pi^3 c^3} \, {\rm e}^{-\frac{\hbar\omega}{k_{\rm B}T}} \int_0^\infty W(\beta)\, d\beta \times {\rm Im}\, \langle i'|\langle f'| \left[\hbar\omega - \hbar\omega_{if} - \Sigma_{if}(\omega,\beta) + \imath\Gamma^{\rm v}_{if}\right]^{-1} |f''\rangle|i''\rangle \quad (1)$$

where $\langle i|\mathbf{r}|f\rangle$ is identified as a dipole matrix-element for the transition probability between initial (n_i, l_i, m_i) and final (n_f, l_f, m_f) states. The ionic microfield strength $\beta = E/E_0$ is normalized to the Holtsmark field E_0, and $\hbar\omega_{if} = E_i - E_f$ is the unperturbed transition energy. The interference correction $\Gamma^{\rm v}_{if}$ for the overlapping line is related to coupling between the initial and final states, the interference contribution vanishes for this transition because the lower state is a s-state and thus not collisionally connected to itself.

The interference term is less important for neutral helium, and is ignored in the dipole approximation, this is not the case for quadrupole approximation of transition [1,20]. However, more accurate calculations are needed for lines involving transitions with high excited states, which are almost hydrogenic states of the helium atom. If the contribution of the lower levels is neglected, then the interference term is zero [21]. Generally the interference contribution is less important for non-hydrogenic line transitions [20]. The function $\Sigma_{if}(\omega,\beta)$ is determined by the self-energy correction $\Sigma_n(\omega,\beta)$ of the initial and the final states

$$\Sigma_{if}(\omega,\beta) = {\rm Re}\big[\Sigma_i(\omega,\beta) - \Sigma_f(\omega,\beta)\big] + \imath\, {\rm Im}\big[\Sigma_i(\omega,\beta) + \Sigma_f(\omega,\beta)\big] \quad (2)$$

where the real part represents the shift $\Delta^{\rm SE}_n$ and the imaginary part gives the width $\Gamma^{\rm SE}_n$ of each state. The electronic and ionic contributions occur in the self-energy. Performing Born approximation with respect to the dynamically screened perturber–radiator potential $V(q)$, the diagonal elements of electronic self-energy operator is obtained as (see Appendix B)

$$\Delta^{\rm SE}_n + \imath\Gamma^{\rm SE}_n = < n|\Sigma^{\rm el}(E_n,\beta)|n >= -\frac{1}{e^2}\int \frac{{\rm d}^3q}{(2\pi)^3} V(q) \sum_\alpha |M_{n\alpha}(\mathbf{q})|^2 \times \int_{-\infty}^{\infty} \frac{{\rm d}\omega}{\pi}[1 + n_{\rm B}(\omega)] \frac{{\rm Im}\,\varepsilon^{-1}(\mathbf{q},\omega+\imath 0)}{E_n - E_\alpha(\beta) - \hbar(\omega+\imath 0)}. \quad (3)$$

Here, the level splitting $(E_\alpha(\beta) \approx E_\alpha)$ due to the microfield has been neglected, $n_{\rm B}(\omega) = \left[\exp(\hbar\omega/k_{\rm B}T) - 1\right]^{-1}$ is the Bose distribution function, approximated by the Boltzmann distribution function for non-degenerated plasma. The sum over principal quantum number α runs from $n-2$ to $n+2$ discrete bound states for the virtual transitions. Dynamic screening is obtained from the imaginary part of the inverse dielectric function $\varepsilon^{-1}(\mathbf{q},\omega)$, for which the random phase

approximation (RPA) is used. The transition matrix-element $M_{n\alpha}(\mathbf{q})$ describes the interaction of the atom with the Coulomb potential through the vertex function, where the Coulomb interaction with the electron-electron-ion triplet depends on the momentum transfer $\hbar\mathbf{q}$ (see Appendix C). The electron wavefunctions for helium are obtained by applying the Coulomb approximation method [22]. In the Born approximation, the electronic contribution is overestimated. Hence, in order to avoid this, we apply the cut-off procedure and add the strong collisions term [1,16,23] instead of the partial summation via the T-matrix. For He I we adopt the cut-off parameter and close electron-radiator collisions term, evaluated according to the semiclassical estimation, see [16,23]. For non-hydrogenic radiator the ionic contribution to the self-energy is related to the quadratic Stark effect and quadrupole interaction [24], further details are given in [15,16].

The above procedure is used to describe the perturbing effect of free electrons on the radiator from the electronic self energy and the interference correction, which gives exactly the same expression as the semiclassical impact approximation of Griem [1], if the term with q^2 is neglected in the argument of delta function as in the classical limit, see Equation (4.5) in [13]. The comparison between the Green's function approach and impact approximation is proved in detail by Kraeft *et al*. [25].

3.1.1. T-Matrix Approach

The electronic contribution can be evaluated again from the effective T-matrix approach which is based on the partial summation. To avoid the cut-off procedure for strong electron-atom collisions, the electronic contribution to shift and width of spectral lines can be treated via partial summation of the three-particle T-matrix. A three-particle propagator (T_3) in the channel of the two-particle bound state and perturbing electron was adopted by Günter [2,26] for calculating the hydrogen L_α line. It can describe weak and strong collisions within static Debye screening. For a non-degenerate plasma, the electronic contribution can be evaluated from scattering amplitudes, characterized by the self energy [19]

$$\Sigma_n^{\mathrm{el}} = -\frac{2}{\pi} n_e \Lambda_{\mathrm{th}}^3 \int_0^\infty dk\, k^2\, e^{-k^2/(k_{\mathrm{B}}T)}\, f_n(0,k). \tag{4}$$

Here, $\Lambda_{\mathrm{th}} = \sqrt{4\pi/(k_{\mathrm{B}}T)}$ is thermal wave length, and $f_n(\theta = 0, k)$ are forward scattering amplitudes of elastic electron scattering at the Debye screened He I for both state initial $(n = i)$ and final $(n = f)$ states, respectively. The singlet $S = 0$ and triplet $S = 1$ channels for scattering are considered for both initial i and final f states. This expression was also found by Baranger [27]. The single electron-atom and -ion scattering problem is studied to provide reliable results for all transitions of interest including elastic, excitation, ionization, and total cross sections [28–30]. Recently, the electron-helium scattering in weakly coupled hot-dense plasmas has been investigated by using the Convergent Close Coupling method (CCC), where the Laguerre basis expansions are applied to obtain fully convergent scattering amplitudes in the close-coupling equations. The screened Coulomb potential or Debye-Hückel potential [31,32] has been employed. This Yukawa-type potential has been used to describe the plasma Coulomb screening effect by formulating a set of close-coupling equations for the T-matrix approach by providing a complete description of the scattering process. The CCC method solves the close-coupling equations in momentum space and uses the T-matrix to determine the cross sections and forward scattering amplitudes for dipole and spin-allowed transitions on the Debye screened neutral helium

atom, The CCC method uses the analytical Born subtraction technique to speed up the convergence of the partial-wave expansion, thus the first Born approximation matrix elements for inelastic scattering is modified. The quantum system involves electron-helium scattering from the ground-state state up to 4f with the correct energies using 153 pseudo-states to describe the scattering, more details are given in [33–35]. Our method gives different results for singlet and triplet scattering channels as well as for scattering at the emitter with initial and final states. Here, we consider only the electron-He forward elastic scattering amplitudes $f(0,k)$ from initial state (n_i, l_i, m_i) to final state (n_f, l_f, m_f) for the self-energies, where n, l, m are the well known principal quantum numbers. Here, the transitions $2S \rightarrow 2S$ and $3P \rightarrow 3P$ are considered for double channel transitions. For a detailed description of the T-matrix calculation see [19].

3.1.2. Microfield Distribution Function

The ionic microfield is considered to be constant during the time of interest of the order of the inverse HWHM of the line, so that a static description of the microfield can be used. In this study, the plasma microfield distribution function is calculated by taking into account the screening and quantum effects of diffraction, the evaluated distribution function is used for calculating line broadening for analyzing the experimental data of Jovićević *et al.* [12]. Processes such as ionization, dissociation, and excitation of bound states occur continuously in plasma and affect plasma properties and its compositions [36]. The distribution of charged particles in the system within the Debye radius r_D is not homogeneous at distances $r < r_D$, although the plasma is electrically neutral as a whole, but at sufficiently small distances the fluctuation of the local electric field affects the plasma kinetic coefficients, optical and thermodynamic properties, *etc*. [37]. According to Ecker and Müller [38] the effective Debye screened field is defined as

$$\vec{E} = \frac{e}{r^3}\vec{r}(1 + r/r_D)e^{-r/r_D} \tag{5}$$

The problem of microfield distribution is formally similar to the problem of determining the chemical potential. This allowed Iglesias [39] to reduce the microfield problem to finding the radial distribution functions (RDF) of some fictitious system with a complex potential energy of interaction. This made the basis for the development of the integral equations method to study the problem of the plasma microfield distribution.

In this paper, we use a method for calculating the distribution function of ionic microfield component $P(E)$ proposed by Iglesias [40]. The advantage of this method is that the distribution function is exactly expressed in terms of a two-body function and does not require knowledge of many-body functions. We use a strongly coupled one component plasmas (OCP) model, *i.e.*, in a fully ionized plasma, in which the electron component forms a homogeneous neutralizing background with N positively charged particles. The microfield distribution function $W(\vec{E})$ is defined as the probability of finding an electric field $\vec{E}$ at a charged point located at $\vec{r}_0$. It is generally expressed in terms of the probability density $P_{N+1}(\vec{r}_0, \vec{r}_1, ..., \vec{r}_N)$ of finding a particular configuration of $(N + 1)$ particles:

$$W(\vec{E}) = \int ... \int \delta(\vec{E} - \sum_{j=1}^{N} \vec{E}_j) P_{N+1}(\vec{r}_0, \vec{r}_1, ..., \vec{r}_N) d\vec{r}_0, d\vec{r}_1, ..., d\vec{r}_N \tag{6}$$

where $\vec{E}_j$ is the electric field, created by $j-$th particle on radiating atoms or ions at $\vec{r}_0$. Assuming the system is isotropic we may introduce Fourier transformation of the function $W(\vec{E})$

$$P(E) = \frac{2E}{\pi}\int_0^\infty l\,T(l)\sin(El)\,dl \tag{7}$$

where $T(l)$ is the characteristic function with a total pair correlation function $h(\vec{r};\lambda)$

$$\ln T(l) = n\int_0^1 d\lambda \int_0^\infty d\vec{r}\,\frac{\imath q\hat{l}\vec{r}}{r^3}h(\vec{r};\lambda) \tag{8}$$

with $\hat{l}$ is a unit vector in the direction of $\vec{l}$, and the introduced parameter λ is a magnitude of the vector $\vec{l}$, while q is the charge of ions, immersed in a neutralizing electron background. The next step is a definition of $h(\vec{r};\lambda)$. The simplest approximation suitable for a Coulomb system is the Debye–Hückel theory. In this approximation we have

$$h(\vec{r};\lambda) \approx \exp\{-\bar{\beta}[1-\frac{\imath\lambda\vec{l}}{q\bar{\beta}}\vec{\nabla}_0]\Phi(r)\} - 1. \tag{9}$$

In [41] with the help of linear response method an effective potential was obtained, which is also used in this paper, by taking in to account both the diffraction effects at short distances and the screening effect at large distances

$$\Phi(r) = -\frac{Z_\alpha e^2}{\sqrt{1-4\lambda_{\alpha e}^2/r_D^2}}\Big(\frac{e^{-Br}}{r} - \frac{e^{-Ar}}{r}\Big) \tag{10}$$

where

$$\begin{aligned} A^2 &= \frac{1}{2\lambda}\Big(1+\sqrt{1-4\lambda_{\alpha e}^2/r_D^2}\Big) \\ B^2 &= \frac{1}{2\lambda}\Big(1-\sqrt{1-4\lambda_{\alpha e}^2/r_D^2}\Big). \end{aligned}$$

The coupling parameter is defined by $\Gamma = \bar{\beta}e^2/r_0$, and

$$r_D = (4\pi n e^2\bar{\beta})^{1/2}\,,\ \bar{\beta} = (k_{\mathrm{B}}T)^{-1}\,,\ r_0 = (4\pi n/3)^{-1/3} \tag{11}$$

where r_0 is the mean particle distance. Here the reduced form of pseudopotential is used

$$-\bar{\beta}\Phi(r) = -\frac{\Gamma}{R}\frac{1}{\sqrt{1-24\Gamma^2/(\pi r_s)}}\Big(e^{-BR} - e^{-AR}\Big) \tag{12}$$

with

$$\begin{aligned} A^2 &= \frac{\pi r_s}{4\Gamma}\Big(1+\sqrt{1-24\Gamma^2/(\pi r_s)}\Big) \\ B^2 &= \frac{\pi r_s}{4\Gamma}\Big(1+\sqrt{1-24\Gamma^2/(\pi r_s)}\Big). \end{aligned}$$

In order to solve Equation (6) numerically, it is better to use the dimensionless field units and to introduce $l^* = E_0 l$. Thus we obtain a formula to calculate the distribution of electric field E^*:

$$\mathcal{P}(E^*) = \frac{2E^*}{\pi}\int_0^\infty dl^*\,l\,T(l^*)\,\sin(E^*\,l^*). \tag{13}$$

By substitution of Equation (9) into Equation (8) yields

$$\begin{aligned} \ln T(l) &= 3\int_0^\infty dR \cdot \exp\left\{\frac{\Gamma}{R}\frac{1}{\sqrt{1-\chi}}(e^{-AR}-e^{-BR})\right\} \\ &\times \frac{R^2}{e^{-BR}(1+BR)-e^{AR}(1+AR)} \end{aligned} \tag{14}$$

where $\chi = 6\Gamma^2/(\pi r_s)$, $R = r/r_0$ and

$$lb(R) = \frac{lq}{r_0}\frac{e^{-BR}(1+BR)-e^{-AR}(1+AR)}{R^2}$$

The one-dimensional integration over R involves the sin transformation in Equation (7), in which $T(l)$ is defined by Equation (8) which is solved numerically.

The microfield distribution function illustrated here is applied for calculating the line profiles to determine the plasma parameters of the measured data by Jovićević *et al.* [12].

3.1.3. Frequency Fluctuation Model

Recently, Calisti *et al.* [18] presented a very fast method to account for ion dynamic effects on atomic spectra in plasmas. This method is based on reformulation for the frequency fluctuation model (FFM), which provides an expression of the dynamic line shapes based on a mixing frequency and the quasistatic Stark profiles. This method allows a very fast and accurate calculation of Stark broadening $I(\omega)$ by taking into account ion-dynamics in this expression

$$I(\omega) \sim \mathrm{Re}\frac{\int \frac{\mathcal{A}(\omega')\,d\omega'}{\gamma+i(\omega-\omega')}}{1-\gamma\int \frac{\mathcal{A}(\omega')\,d\omega')}{\gamma+i(\omega-\omega')}}. \tag{15}$$

Here, $\mathcal{A}(\omega)$ is the area-normalized line profile in quasistatic limit, evaluated from Equation (1), the inverse state lifetime $\gamma = v_{\mathrm{th}}/d$ is defined by ion thermal velocity of perturbers $v_{\mathrm{th}} = \sqrt{8k_{\mathrm{B}}T/(\pi m_i)}$ and the mean distance between ions $d = (4\pi n_i/3)^{-1/3}$, where m_i and n_i are the mass and density of perturbing ions, respectively.

3.2. Classical Molecular Dynamics Simulations

Spectral line shapes $I(\Delta\omega)$ are also calculated using molecular dynamics (MD) simulations. Using these simulations, the dynamics of the particles in the plasma is reproduced numerically in the computer and the electric field sequences suffered by the emitters are obtained. These field sequences are taken to the differential equations that permit to calculate the emitter evolution, and the final profiles are obtained as the Fourier transform of an average of the emitter dipole-moment autocorrelation function [42].

$$I(\Delta\omega) = \mathrm{Re}\frac{1}{\pi}\int_0^\infty dt\,\{C(t)\}e^{i\Delta\omega t} \tag{16}$$

$$C(t) = \mathrm{tr}[\mathbf{D}(t)\cdot\mathbf{D}(\mathbf{0})\,\rho] \tag{17}$$

$$D(t) = U^+(t)\,\mathbf{D}(0)\,U(t) \tag{18}$$

where ρ is the equilibrium density-matrix operator, D is the dipole operator for the radiating system, and the symbols $\{\}$ mean an average over a large number of simulated individual processes obtained in order

to have a representative sampling of the electric fields in the plasma. $U(t)$ is the emitter time evolution operator that obeys Schrödinger equation

$$\imath\hbar\frac{d}{dt}U(t) = H(t)U(t) = \Big(H_0 + q\mathbf{E}(t)\cdot\mathbf{R}\Big)U(t) \tag{19}$$

where the Hamiltonian $H(t)$ includes the structure of the emitter states without perturbation H_0, and the action of the perturbers through the dipole interaction with the electric field $\mathbf{E}(t)$ at the emitter location [43]. For a specific line transition, two groups of states are considered, the upper and lower group of states of the transition. If the difference in energy of those groups is large enough in comparison with the average energy of the collisions in the plasma, then we can assume that both groups of states evolve independently though undergoing the same sequence of perturbing electric field, which is known as the no-quenching approximation. The simulations used in this work consider that the perturbers are classical point independent particles that move along straight line trajectories with constant speeds according to the Maxwell distribution corresponding to their equilibrium temperature. Correlation effects between perturbers are taken into account considering Debye screened electric fields. The relative movement of the heavy perturbers and the emitter is taken into account using the reduced mass of the emitter-perturber pair according to the μ-ion model [44]. This simulation technique is designed to guarantee that the density of particles within the simulation sphere is kept constant along the simulation and that both the spatial distribution of particles and the velocities distribution are kept stationary [9]. On the other hand, this technique allows us to consider non-equilibrium plasmas [45], and can also be applied to non-homogeneous plasmas [46,47]. However, for strongly interacting plasmas (large plasma coupling parameter) or charged emitters, MD simulations accounting for the interactions between all the particles in the plasma (*i.e.*, including the emitter) are required [48,49], though for the calculations in this work the independent particles technique was accurate enough. More details of the calculation can be seen in [11].

4. Results and Discussions

In this study, we present several theoretical approaches for calculating He I line shapes. The plasma parameters are inferred by comparing our results with the experimental measurement of Jovićević *et al.* [12]. The measured profile is compared with the theoretical profiles at $T = 3.3\times10^4$ K for two values of electron densities $n_e = 5.2\times10^{22}\,\mathrm{m}^{-3}$ and $n_e = 4.58\times10^{22}\,\mathrm{m}^{-3}$, respectively. In [12] the experimental He I 3889 Å line broadening was fitted by using the $j_{AR}(x)$ line profiles generated on the assumption of electron impact broadening combined with broadening by quasistatic ion field using the ST of Griem [1]. The electron density of $n_e = 4.8\times10^{22}\ \mathrm{m}^{-3}$ with an estimated uncertainty of $\pm10\%$ was determined from the line broadening, while the electron temperature of $T = 3.3\times10^4$ K with an uncertainty of $\pm12\%$ was estimated by using the relative intensities of O II impurity lines.

In our quantum statistical approach electrons and ions are treated separately. Green's function is applied for calculating the electronic contribution from Equation (3), while the dominant ionic contribution arises from the quadratic Stark effect and quadrupole interaction [15,16]. First, the ionic contribution is determined in the quasistatic approximation by using the calculated microfield

distribution function in Section 3.1.2, then the new FFM formulation [18] is adopted to account for the fluctuation of the microfield on the spectral line shapes. The dynamic effects of the ionic motion are taken into account by substituting the area-normalized static profile into Equation (15). The result is displayed in Figure 1, which compares measured and theoretical profiles. Since the authors of the original experimental paper [12] did not mention any measurement of absolute line shift, we displaced the calculated line profiles to the unperturbed wavelength $\lambda_0 = 3888.65$ Å in Figures 1–3 to determine the free electron density n_e from the line width.

Figure 1. The calculated He I (2^3S–3^3P) line profiles in dynamically screened Born approximation by including ion dynamics in the FFM . Comparison is made with the measured data by Jovićević *et al.* [12] at $T = 3.3 \times 10^4$ K. The profiles are plotted at the unperturbed transition wavelength $\lambda_0 = 3888.65$ Å, and the shift of profiles are shown.

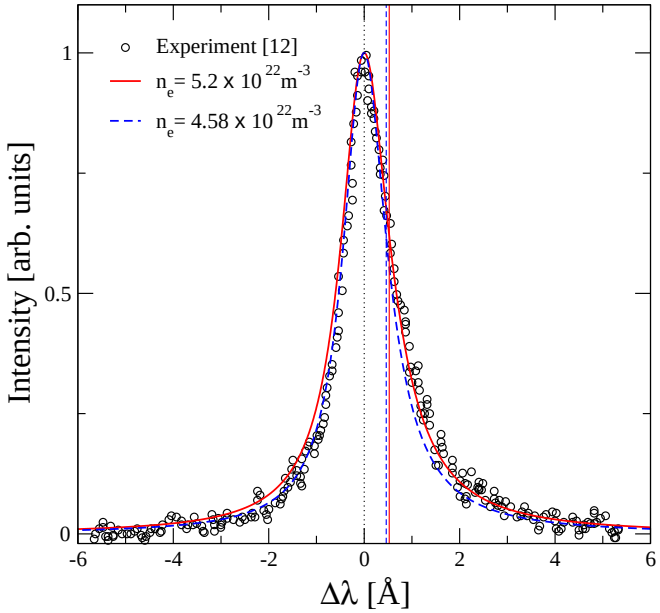

The electronic contribution is recalculated via the T-matrix by applying the CCC method in order to describe the strong electron-helium collisions within the Debye static screening model [34]. Both real and imaginary part of forward scattering amplitudes are substituted in Equation (4) to provide electronic shift and width [19]. In contrast to the Born approximation, the contribution of each state is different for different values of the magnetic quantum number $|m| = 0, 1$. Furthermore, an average over different spin-scattering channels $S = 0$ and $S = 1$ has been done. The Stark profiles are calculated in the quasistatic approximation from Equation (1) by using the T-matrix approach for electron-emitter collisions, The dynamic profiles are evaluated from Equation (15) and illustrated in Figure 2. It may be seen that the electron density $n_e = 5.2 \times 10^{22}\,\mathrm{m}^{-3}$ gives better agreement with the experimental profile in Figures 1 and 2.

Results from simulations are presented in Figure 3. Dynamic profiles show very good agreement with the measured profile for the inferred plasma density $n_e = 4.58 \times 10^{22}\,\mathrm{m}^{-3}$ and temperature $T = 3.3 \times 10^4$ K. In Table 1, numerical results of the shift and FWHM from our theories are given. We compare the broadening parameters in the dynamically screened Born approximation, the T-matrix approach, and MD simulations for interacting particles.

Figure 2. Comparison between the measured [12] and calculated line shapes of He I (2^3S–3^3P) using the T-matrix approach with ion dynamics in the FFM at $T = 3.3 \times 10^4$ K. The profiles are given at the unperturbed transition wavelength $\lambda_0 = 3888.65$ Å, and the shift of profiles are shown.

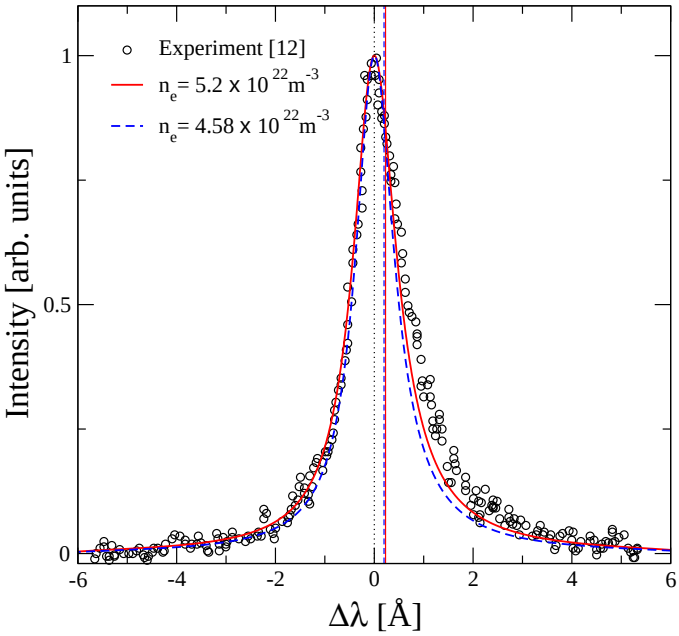

Figure 3. The calculated He I (2^3S–3^3P), line profiles from MD simulations compared with the experimental result of Jovićević *et al.* [12] at $T = 3.3 \times 10^4$ K. The profiles are given at the unperturbed transition wavelength $\lambda_0 = 3888.65$ Å, and the shift of profiles are shown.

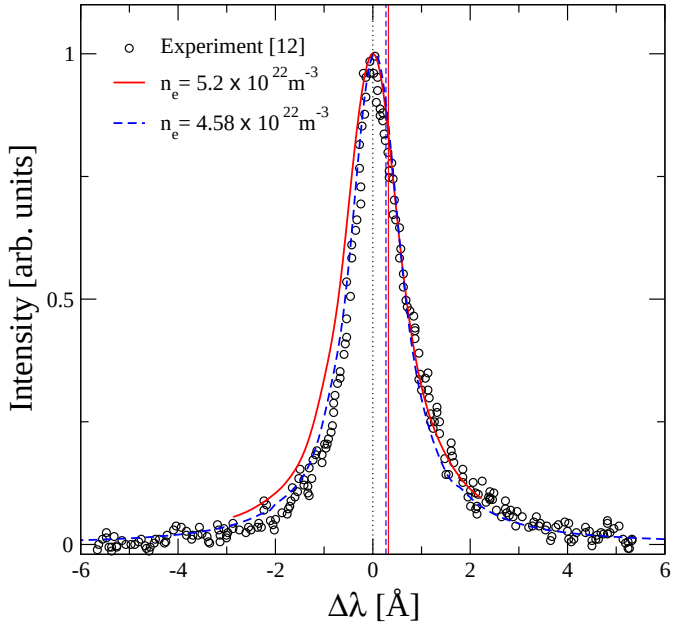

Figure 4. The shift of He I 3889 Å *vs.* electron density. Comparison between our calculated data and the experimental results are shown. The electron temperature is given for the corresponding T-matrix data points.

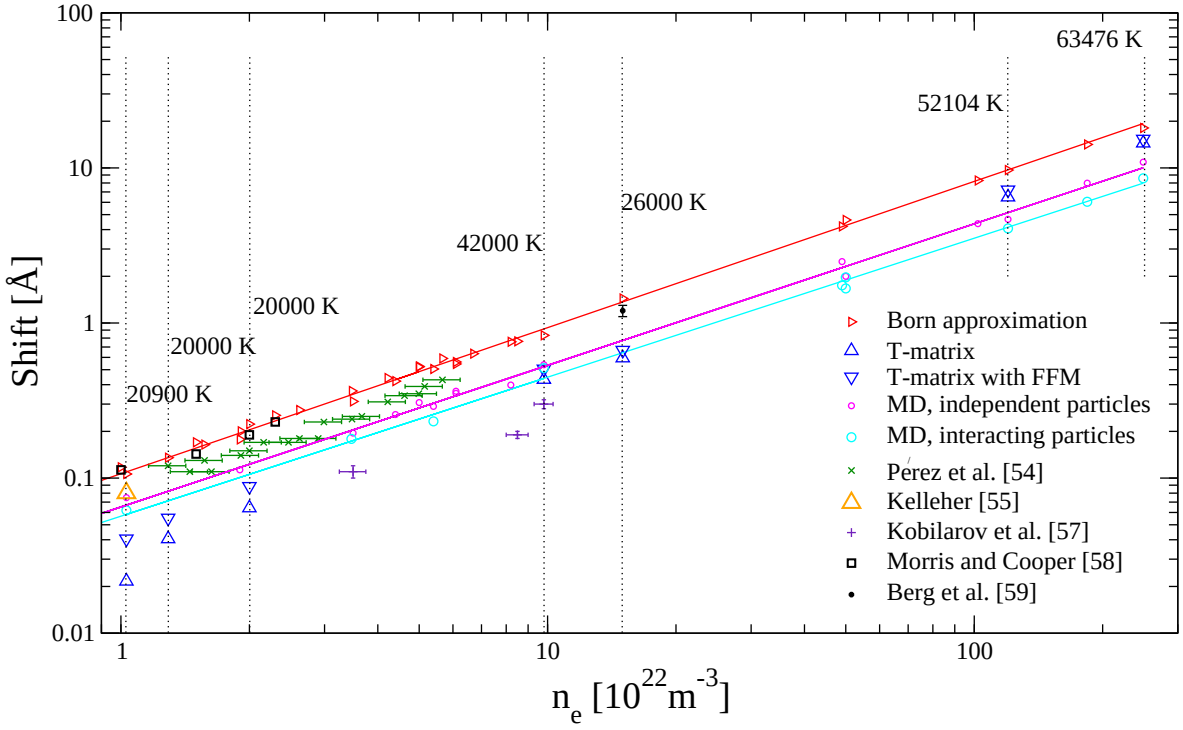

Ion dynamics (FFM) are included in the Born approximation and the T-matrix approach, the dynamic effects lead to further shift. The shift is significantly affected by including strong collisions via the T-matrix and ion-dynamics, while the dynamic profiles appear slightly broadened compared to the static profile. The calculated line shift for different values of n_e is illustrated in Figures 1–3 as well. Note, that the shift of this line is red, towards larger wavelengths with respect to the unperturbed transition line at λ_0. An example of the line measurement can be seen also in [50].

Table 1. Theoretical calculations of shift and FWHM of the He I 3889 Å line are illustrated in [Å], to analyze the experimental result of Jovićević *et al.* [12]. The calculated values correspond to dynamically screened Born approximation (quasistatic/FFM), T-matrix approach (quasistatic/FFM) and MD simulations at $T = 3.3 \times 10^4$ K.

n_e 10^{22} m^{-3}	Shift [Å]			FWHM [Å]		
	Born	T-Matrix	MD	Born	T-Matrix	MD
5.2	0.483/0.523	0.178/0.228	0.32	1.245/1.278	1.038/1.087	1.402
4.58	0.427/0.462	0.147/0.197	0.269	1.094/1.123	0.914/0.965	1.245

The illustrated approaches can provide the shift and full width at half maximum (FWHM) in a wide range of n_e and T. The comparison with different measurements for shift and FWHM as a function of electron density $n_e \approx (10^{22} - 10^{24})\mathrm{m}^{-3}$ in temperature range $T \approx (2 - 6) \times 10^4$ K are shown in Figures 4 and 5, respectively. The microfield distribution function of Hooper [51] is used in both the

Born approximation and the T-matrix method for evaluating the Stark parameters in Figures 4 and 5 [19]. However, outside the validity range of Hooper's approach, we used the fit formula of Potekhin *et al.* [52] in our previous calculations in [19,53], which is based on Monte Carlo simulations and is appropriate for strongly coupled plasmas as well. The calculated FWHM in the T-matrix approach shows good agreement with the MD simulations data, especially at high densities. The ion dynamics slightly affects the width. However, the shift is rapidly reduced at low electron densities, and the discrepancy can be seen in contrast to MD simulations, but still the contribution of FFM is more pronounced in this region. The shift of this line is overestimated in the Born approximation compared to both the T-matrix method and MD simulations. The correlation between perturbers tends to decrease the line shift and width at high electron densities for interacting particles. In Figures 4 and 5 the comparison is made with the following experiments: The measurement by Pérez *et al.* [54] was done in a low-pressure pulsed arc, in the plasma density range of $n_e = (1-6) \times 10^{22}\,\mathrm{m}^{-3}$ and temperature interval of $T = (0.8-3) \times 10^4$ K with a mean value of 2×10^4 K . The error bar of n_e was $\pm 10\%$, and uncertainty in the temperature evaluation was about 20%. The experimental result of Kelleher [55] was obtained in a helium plasma generated in a wall-stabilized arc, with $n_e = 1.03 \times 10^{22}\,\mathrm{m}^{-3}$ and $T_e = 2.09 \times 10^4$ K. Recently, the FWHM of the same transition line was measured by Gao *et al.* [56] from a helium arc for the density range $n_e = (0.5-4) \times 10^{22}\,\mathrm{m}^{-3}$ at $T = 2.3 \times 10^4$ K. The reported result by Kobilarov *et al.* [57] from a pulsed low-pressure arc at $n_e = (2-10) \times 10^{22}\,\mathrm{m}^{-3}$ and $T = (3.1-4.2) \times 10^4$ K are included. Furthermore, values for the shift measured by Morris and Cooper [58] within the density range $n_e = (0.6-2.3) \times 10^{22}\,\mathrm{m}^{-3}$ and $T = (1-1.6) \times 10^4$ K are shown. The Stark parameters of this line were also measured by Berg *et al.* [59] at $n_e = 1.5 \times 10^{22}\,\mathrm{m}^{-3}$ and $T_e = 2.6 \times 10^4$ K. The measured widths by Milosavljević and Djeniže [60] are included as well, by using a linear low-pressure pulsed arc. The measured electron density and temperature were in the ranges of $(4.4-8.2) \times 10^{22}\,\mathrm{m}^{-3}$ and $(1.8-3.3) \times 10^4$ K with error bars $\pm 9\%$ and $\pm 10\%$, respectively. Furthermore, a comparison is made with the measurement of Soltwisch and Kusch [61], a wall-stabilized quasistationary pulsed discharge was used as a homogeneous plasma source. The spectra were recorded in a single shot, and the electron density range of $(0.7-1.2) \times 10^{23}\,\mathrm{m}^{-3}$ was determined from the plasma reflectivity at two different wavelengths. The estimation of the temperature was about 2×10^4 K.

As shown in Figure 5, the T-matrix approach always gives a smaller FWHM than the Born approximation. This trend leads to a better agreement with the MD simulations results for interacting particles. For the data of Pérez *et al.* [54], the calculated width in the T-matrix approach agrees very well with the result of the Born approximation. However, the measurement may be influenced by self-absorption, as mentioned in [54], and then the measured widths may be overestimated. At $n_e = 9.8 \times 10^{22}\,\mathrm{m}^3$, the width in the Born approximation shows a very good agreement with both measurement and MD simulations for independent particle data. However, the results of T-matrix approach and MD simulations for interacting particles give slightly lower values than the experiment data. At the highest measured density, the FWHM of theories is below that of Berg *et al.* [59]. Good agreement is found between the MD simulations result and T-matrix approach. However, the shift of this line is overestimated in the Born approximation, where, the strong collisions with large momentum transfer are not treated appropriately, while the perturbation theory breaks down at small distances and the perturbative expansion has to be avoided [20].

Figure 5. The FWHM of He I 3889 Å as a function of electron density. Our theoretical approaches are compared with the experiments results.

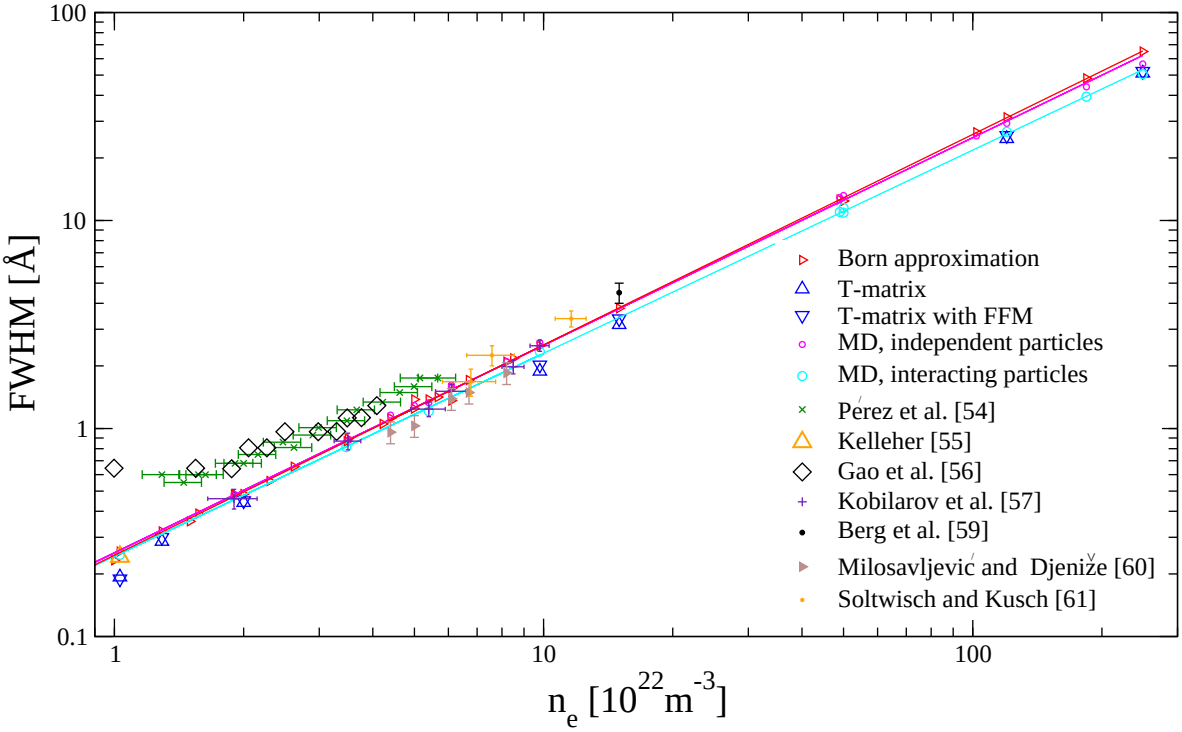

5. Conclusions

Spectral line shapes for He I are investigated theoretically in dense plasmas, the comparison is made with the measurements of Jovićević *et al.* [12] for diagnostic purposes. Free electron-emitter collisions are considered within both the Born approximation, and the T-matrix approach while ions are treated by the quasistatic approximation. The electronic contribution to the shift and width is computed by thermodynamic Green's function by using Born approximation, which is the main contribution to the line broadening. Dynamic screening of the electron-atom interaction is included, which is a collective, many-particle effect. In contrast to ST, this effect modifies the broadening parameters with increasing free electron density, causing a non-linear behavior, where the plasma oscillations become relevant, see Figures 4 and 5. A cut-off procedure for strong collisions is used according to Griem [1], while the second-order Born approximation overestimated the electronic contribution and the strong collisions term are added [23]. The Coulomb approximation is employed to evaluate the wavefunctions of helium. The accuracy of this approximation was approved for He-like ion by comparing our result with the Hartree-Fock wavefunctions, thus the radial part of transition matrix-element from various approaches were compared in [62].

Then the electron-emitter interaction is investigated again by elastic scattering amplitudes in Debye plasmas from a two-particle T-matrix approach by using the close-coupling equations. The Debye–Hückel potential significantly affects the bound states and scattering processes of the metastable states. The result is improved by treating strong electron-helium collisions consistently within T-matrix approach and better agreement can be seen with the measurement than the Born approximation, especially for the line shift. The contribution of perturbing ions is taken into account in a quasistatic

approximation, with both quadratic Stark effect and quadrupole interaction. The perturbing ionic microfield is considered as a static field during the radiation. The calculated spectral line shapes in the static limit are modified by applying the FFM for both the Born approximation and T-matrix approach, which provides the dynamic line shapes and leads to further broadening [18]. In addition, MD simulations are used for comparison with the experiments and the analytically obtained profiles.

The shift of this line is over estimated in Born approximation even with a cut-off procedure and better agreement can be seen with the screened T-matrix approach and MD simulations. The FWHM of all theoretical approaches are in good agreement with the experimental result.

Acknowledgments

The authors thank the anonymous referees for their very helpful comments and suggestions. This work was supported by the German Research Foundation DFG within SFB 652. The support of the Australian Research Council, the Australian National Computational Infrastructure Facility, and its Western Australian node iVEC are gratefully acknowledged.

Author Contributions

B.O. did the quantum statistical calculations and analysis, M.Á.G and M.A.G did the computer simulations, T.S.R., M.C.J., and K.N.D. calculated the microfield distribution function, M.C.Z., D.V.F., and I.B. calculated the scattering amplitudes.

Appendix A: Spectral Line Profile

The Green's function methods provide a systematic approach to correlation functions in many-body system. The theory includes correlations and quantum effects of the many-body system. The line broadening is proportional to the imaginary part of the inverse dielectric function of the plasma. The two-particle Green's function is used to calculate the line shapes. Recently, further improvements of this approach have been made by Günter *et al.* [2], Hitzschke *et al.* [13], and Röpke *et al.* [63]. Optical properties of many-particle systems are described by the dielectric function $\varepsilon(\mathbf{q},\omega)$ based on Green's function theory, which is the response of the medium to an external electromagnetic field. The dielectric tensor can be divided into transversal t and longitudinal l parts, depending on wavenumber $\mathbf{q}$ and frequency ω. $\varepsilon_{\mathrm{l}}(\mathbf{q},\omega)$ is related to the polarization function $\Pi(\mathbf{q},\omega)$,

$$\varepsilon_{\mathrm{l}}(\mathbf{q},\omega) = 1 - V(q)\,\Pi(\mathbf{q},\omega) \tag{20}$$

where $V(q) = e^2/(\epsilon_0 q^2)$ is the Fourier transformed Coulomb potential. Starting from the relation of the absorption coefficient $\alpha(\omega)$ and the index of refraction $n(\omega)$, the transverse dielectric function $\varepsilon_{\mathrm{t}}(\mathbf{q},\omega)$ in the long wavelength limit $q^{-1} = c/\omega \to 0$ reads

$$\lim_{\mathbf{q}\to 0} \varepsilon_{\mathrm{t}}(\mathbf{q},\omega) = [n(\omega) + \frac{\imath c}{2\omega}\alpha(\omega)]^2. \tag{21}$$

In the visible region where the wavelength λ is large compared with the atomic dimension a_{B}, the transverse and the longitudinal part of dielectric function coincide

$$\lim_{\mathbf{q}\to 0} \varepsilon_{\mathrm{t}}(\mathbf{q},\omega) = \lim_{\mathbf{q}\to 0} \varepsilon_{\mathrm{l}}(\mathbf{q},\omega) = \lim_{\mathbf{q}\to 0} \varepsilon(\mathbf{q},\omega). \tag{22}$$

The absorption coefficient is proportional to the imaginary part of the dielectric function

$$\begin{aligned} \alpha(\omega) &= \frac{\omega}{c\, n(\omega)} \lim_{\mathbf{q}\to 0} \mathrm{Im}\, \varepsilon(\mathbf{q},\omega) \\ n(\omega) &= \frac{1}{\sqrt{2}} \lim_{\mathbf{q}\to 0} \left\{ \mathrm{Re}\, \varepsilon(\mathbf{q},\omega) + \left[(\mathrm{Re}\, \varepsilon(\mathbf{q},\omega))^2 + (\mathrm{Im}\varepsilon(\mathbf{q},\omega))^2 \right]^{1/2} \right\}^{1/2}. \end{aligned} \tag{23}$$

In the case of thermal equilibrium, the absorption coefficient $\alpha(\omega)[\mathrm{cm}^{-1}]$ is related to the emission coefficient $j(\omega)[\mathrm{erg\,cm^{-3}\,s^{-1}\,Hz^{-1}\,ster^{-1}}]$ by Kirchhoff's law [64]. The emission coefficient is defined as the number of photons with frequency between ν and $(\nu + d\nu)$ emitted per unit time per unit volume per unit frequency interval

$$j(\omega) = \alpha(\omega) B(\omega, T) \tag{24}$$

$$B(\omega, T) = \frac{\hbar\omega^3}{4\pi^3 c^2} \left[\exp(\frac{\hbar\omega}{k_{\mathrm{B}} T}) - 1 \right]^{-1} \tag{25}$$

where $B(\omega, T)$ is the black body radiation, defined in intensity units per steradian $[\mathrm{erg\,cm^{-2}\,s^{-1}\,Hz^{-1}\,ster^{-1}}]$. In an optically thin plasma, $j(\omega)$ can be approximated to the specific intensity (surface brightness) $I(\omega)$. The dielectric function itself can be determined from the polarization function according to Equation (20). The medium modifications of spectral line shapes can be described in a systematic way from the bound–bound two-particle polarization function $\Pi_2(\mathbf{q}, \omega)$ [2,13,25,65]. From Equations (20), (23) and (24) the line emission is given by

$$j(\omega) = \frac{\omega^4}{4\pi^3 c^3 n(\omega)} \left[\exp(\frac{\hbar\omega}{k_{\mathrm{B}} T}) - 1 \right]^{-1} \lim_{q\to 0} \mathrm{Im}\, \varepsilon(\mathbf{q}, \omega). \tag{26}$$

Assuming $n(\omega) = 1$ for $\omega \gg \omega_{\mathrm{pl}}$, and $q \to 0$

$$j(\omega) \approx \frac{\omega^4}{4\pi^3 c^3} \exp(-\frac{\hbar\omega}{k_{\mathrm{B}} T}) \lim_{q\to 0} \mathrm{Im}\, \Pi(\mathbf{q}, \omega). \tag{27}$$

The polarization function $\Pi_2(\mathbf{q}, \omega)$ is related to the dipole–dipole autocorrelation function, which describes the pressure broadening (Stark broadening) [66]. A systematic treatment of the two-particle polarization function can be performed via Green's function

$$\Pi_2(\mathbf{q}, \omega) = \sum_{i\,f} |M^0_{if}(\mathbf{q})|^2 \frac{[g(\omega_i) - g(\omega_f)]}{\hbar\omega - \hbar\omega_{if} - \Delta_{if} - \imath\Gamma_{if} + \imath\Gamma^{\mathrm{v}}_{if}} \tag{28}$$

thus the imaginary part of this expression is substituted in Equation (26), which describes the spectral line shapes, see Equation (1). The two-particle Bose distribution function can be approximated by the Boltzmann distribution function for non-degenerated plasmas

$$g_{e\,i}(\omega) = \frac{1}{e^{\bar\beta(\omega - \mu_e - \mu_i)} - 1} \approx \frac{1}{4}\, n_{e\,i}\, \Lambda^3_{e\,i}\, e^{-\bar\beta\omega} \tag{29}$$

where $\Lambda_{ei} = \sqrt{2\pi\bar\beta/m_i}$ is the thermal wavelength, m_i is the mass of radiator, and $\bar\beta = 1/(k_{\mathrm{B}} T)$. The pressure line broadening is achieved by substituting Equation (28) into Equation (27) and averaging over the microfiled distribution function, see Eq. (1). The Rydberg units ($\hbar = 2m_e = e^2/2 = 1$) are used throughout this paper.

Appendix B: Electronic Self-energy

The electronic self-energy Σ_2 has been calculated from the quantum-statistical many-particle approach, by using the two-particle Green's function G_2^0 for the radiating atom in the momentum $\mathbf{P}+\mathbf{q}$ and frequency representation $\Omega_\lambda - \omega_\mu$ [15], where Ω_λ and ω_μ are the bosonic the Matsubara frequency. The statistical information on temperature and chemical potential contains in the definition of the Matsubara frequency. The correction self-energy is proportional to the free electron density, given in dynamically screened Born approximation [67,68]. The self-energy is evaluated be solving this diagram

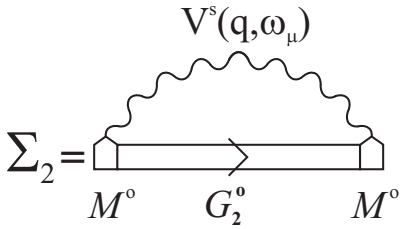

$$\Sigma_2(n,n',\mathbf{P},\Omega_\lambda) \;=\; \frac{1}{-\imath\beta}\sum_{q,\mu,\alpha} M^0_{n\alpha}(\mathbf{q})\, V^s(q,\omega_\mu)\, G_2(\alpha,\mathbf{P}+\mathbf{q},\Omega_\lambda-\omega_\mu) M^0_{\alpha n'}(-\mathbf{q}) \tag{30}$$

where $M^0_{n\alpha}(\mathbf{q})$ is the matrix-element for virtual transitions from the considered state to the excited state, with principal quantum number n,α, see Appendix C. The dynamically screened potential $V^s(q,\omega_\mu)$ for the radiator-electron interaction is represented by the spectral function of the dielectric function $\varepsilon(\mathbf{q},\omega)$

$$V^s(q,\omega_\mu) = V(q) + V(q)\int_{-\infty}^{\infty}\frac{d\omega}{\pi\hbar}\frac{\mathrm{Im}\,\varepsilon^{-1}(\mathbf{q},\omega+\imath 0)}{\omega-\omega_\mu}. \tag{31}$$

The first term in $V^s(q,\omega_\mu)$ is neglected, which leads to the exchange Fock self-energy, whereas the second term is the correction part. The Matsubara summation $\sum_\mu$ can be represented as a contour integral in the complex plane [67]. After performing the Matsubara frequency summation, the real and imaginary part of the diagonal electronic self-energy can be obtained [15,63,69].

Appendix C: Matrix-Element

The transition matrix-element $M_{n\alpha}(\mathbf{q})$ describes the interaction of the atom with the Coulomb potential through the vertex function. In lowest order, they are determined by the atomic eigenfunctions ψ_n. For helium, the Coulomb interaction with an electron-electron-ion triplet depends on the momentum transfer $\hbar\mathbf{q}$, this can be represented for helium and hydrogen by these diagrams [2,25,68,70].

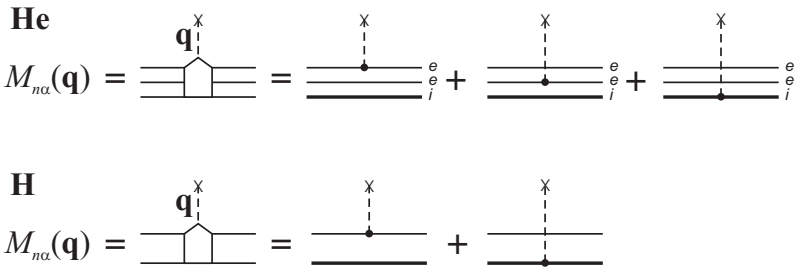

The matrix-element for hydrogen can be written as

$$M_{n\alpha}(\mathbf{q}) = \imath\, e \sum_{\mathbf{p}_e,\mathbf{p}_i} \psi^*_n(\mathbf{p}_e,\mathbf{p}_i)\Big[\, Z_n\;\psi_\alpha(\mathbf{p}_e,\mathbf{p}_i+\mathbf{q}) - \;\psi_\alpha(\mathbf{p}_e+\mathbf{q},\mathbf{p}_i)\Big] \tag{32}$$

However, the helium matrix-element can be approximated by hydrogen, while the outer electron is screened by the inner electron. Here, the states closely adjacent to n are identified by α, and Z_n is the ion charge. In an adiabatic approximation, the ion is much heavier than the electron $m_i \gg m_e$, therefore the relative momentum is approximated by the momentum of electron

$$\mathbf{p} = \frac{m_i \mathbf{p}_e - m_e \mathbf{p}_i}{m_e + m_i} \approx \mathbf{p}_e$$

$$M_{n\alpha}(\mathbf{q}) = \imath\, e \sum_{\mathbf{p}} \psi_n^*(\mathbf{p}) \Big[Z_n\, e\, \psi_\alpha\left(\mathbf{p}\right) - e\, \psi_\alpha\left(\mathbf{p}+\mathbf{q}\right) \Big]. \tag{33}$$

After Fourier transformation of the above relation, and expanding the exponential term into spherical harmonics,

$$M_{n\alpha}(\mathbf{q}) = \imath\, e \left[Z_n\, \delta_{n\alpha} - \int \mathrm{d}^3 r\; \psi_n^*(\mathbf{r})\; \mathrm{e}^{\imath \mathbf{q}\cdot\mathbf{r}}\; \psi_\alpha(\mathbf{r}) \right] \tag{34}$$

$$\mathrm{e}^{\imath \mathbf{q}\cdot\mathbf{r}} = 4\pi \sum_{l=0}^{\infty} \sum_{m=-l}^{l} \imath^l j_l(qr) Y_{lm}^*(\Omega_q) Y_{lm}(\Omega_r)$$

where $j_l(qr)$ is the spherical Bessel function [71], a multipole expansion can be derived, e.g., $l = 0, 1, 2$ give the monopole, dipole and quadrupole contribution of the radiator-electron interaction, respectively. In the long wavelength limit $q \to 0$ for bound–bound transitions, the dipole approximation is valid, where the q-integral is dominated by the small q region [20].

Conflicts of Interest

The authors declare no conflict of interest.

References

1. Griem, H.R. *Spectral Line Broadening by Plasmas*; Academic Press: New York, NY, USA, 1974.
2. Günter, S.; Hitzschke, L.; Röpke, G. Hydrogen spectral lines with the inclusion of dense-plasma effects. *Phys. Rev. A* **1991**, *44*, 6834–6844.
3. Frisch, U.; Brissaud, A. Theory of Stark broadening soluble scalar model as a test. *J. Quant. Spectrosc. Radiat. Transf.* **1971**, *11*, 1753–1766.
4. Seidel, J. Hydrogen Stark Broadening by Model Electronic Microfields. *Z. Naturforschung A* **1977**, *32a*, 1195–1206.
5. Seidel, J. Effects of Ion Motion on Hydrogen Stark Profiles. *Z. Naturforschung A* **1977**, *32a*, 1207–1214.
6. Stehlé, C.; Hutcheon, R. Extensive tabulations of Stark broadened hydrogen line profiles. *Astron. Astrophys. Suppl. Ser.* **1999**, *140*, 93–97.
7. Talin, B.; Calisti, A.; Godbert, L.; Stamm, R.; Lee, R.W.; Klein, L. Frequency-fluctuation model for line-shape calculations in plasma spectroscopy. *Phys. Rev. A* **1995**, *51*, 1918–1928.
8. Stamm, R.; Smith, E.W.; Talin, B. Study of hydrogen Stark profiles by means of computer simulation. *Phys. Rev. A* **1984**, *30*, 2039–2046.
9. Gigosos, M.A.; Cardeñoso, V. New plasma diagnosis tables of hydrogen Stark broadening including ion-dynamics. *J. Phys. B Atom. Mol. Opt. Phys.* **1996**, *29*, 4795–4838.

10. Gigosos, M.A.; González, M.A. Stark broadening tables for the helium I 447.1 line. Application to weakly coupled plasmas diagnostics. *Astron. Astrophys.* **2009**, *503*, 293–299.
11. Gigosos, M.A.; Djurovic, S.; Savic, I.; GonzÃąlez-Herrero, D.; Mijatovic, Z.; Kobilarov, R. Stark broadening of lines from transition between states $n = 3$ to $n = 2$ in neutral helium. An experimental and computer-simulation study. *Astron. Astrophys.* **2014**, *561*, A135:1–A135:13.
12. Jovićević, S.; Ivković, M.; Zikic, R.; Konjević, N. On the Stark broadening of Ne I lines and static *vs*. ion impact approximation. *J. Phys. B Atom. Mol. Opt. Phys.* **2005**, *38*, 1249–1259.
13. Hitzschke, L.; Röpke, G.; Seifert, T.; Zimmermann, R. Green's function approach to the electron shift and broadening of spectral lines in non-ideal plasmas. *J. Phys. B Atom. Mol. Opt. Phys.* **1986**, *19*, 2443–2456.
14. Günter, S. *Optische Eigenschaften Dichter Plasmen.* Habilitation thesis, Rostock University: Rostock, Germany, 1995.
15. Sorge, S.; Wierling, A.; Röpke, G.; Theobald, W.; Sauerbrey, R.; Wilhein, T. Diagnostics of a laser-induced dense plasma by Hydrogen-like Carbon spectra. *J. Phys. B Atom. Mol. Opt. Phys.* **2000**, *33*, 2983–3000.
16. Omar, B.; Günter, S.; Wierling, A.; Röpke, G. Neutral helium spectral lines in dense plasmas. *Phys. Rev. E* **2006**, *73*, 056405:1–056405:13.
17. Günter, S.; Könies, A. Shifts and asymmetry parameters of hydrogen Balmer lines in dense plasmas. *Phys. Rev. E* **1997**, *55*, 907–911.
18. Calisti, A.; Mossé, C.; Ferri, S.; Talin, B.; Rosmej, F.; Bureyeva, L.A.; Lisitsa, V.S. Dynamic Stark broadening as the Dicke narrowing effect. *Phys. Rev. E* **2010**, *81*, 016406:1–016406:6.
19. Lorenzen, S.; Omar, B.; Zammit, M.C.; Fursa, D. V.; Bray I. Plasma pressure broadening for few-electron emitters including strong electron collisions within a quantum-statistical theory. *Phys. Rev. E* **2014** , *89*, 023106:1–023106:13.
20. Hitzschke, L.; Günter, S. The influence of many-particle effects beyond the Debye approximation on spectral line shapes in dense plasmas. *J. Quant. Spectrosc. Radiat. Transf.* **1996**, *56*, 423–441.
21. Beauchamp, A.; Wesemael, F.; Bergeron, P. Spectroscopicstudies of tudies DB white dwarfs: Improved Stark profiles for optical transitions of neutral helium. *Astrophys. J. Suppl. Ser.* **1997**, *108*, 559–573.
22. Bates D. R.; Damgaard, A. The calculation of the absolute strengths of spectral lines. *Phil. Trans. Roy. Soc. Lond. A* **1949**, *242*, 101–122.
23. Griem, H.R.; Baranger, M.; Kolb, A.C.; Oertel, G. Stark broadening of neutral helium lines in a plasma. *Phys. Rev.* **1962**, *125*, 177–195.
24. Halenka, J. Asymmetry of hydrogen lines in plasmas utilizing a statistical description of ion-quadruple interaction in Mozer-Baranger limit. *Z. Phys. D* **1990**, *16*, 1–8.
25. Kraeft, W.-D.; Kremp, D.; Ebeling, W.; Röpke, G. *Quantum Statistics of Charged Particle Systems*; Akademie-Verlag: Berlin, Germany, 1986.
26. Günter, S. Contributions of strong collisions in the theory of spectral lines. *Phys. Rev. E* **1993**, *48*, 500–505.
27. Baranger, M. General impact theory of pressure broadening. *Phys. Rev.* **1958**, *112*, 855–865.

28. Bray, I.; Stelbovics, A.T. Convergent close-coupling calculations of electron-hydrogen scattering. *Phys. Rev. A* **1992**, *46*, 6995–7011.
29. Fursa, D.V.; Dmitry V.; Bray, I. Calculation of electron-helium scattering. *Phys. Rev. A* **1995**, *52*, 1279–1297.
30. Bray, I.; Fursa, D.V.; Kadyrov, A.S.; Stelbovics, A.T.; Kheifets, A.S.; Mukhamedzhanov, A.M. Electron- and photon-impact atomic ionisation. *Phys. Rep.* **2012**, *520*, 135–174.
31. Debye, P.; Hückel, E. *Phys. Zeitschrift* **1923**, *24*, 185–206.
32. Kardar, M. *Statistical Physics of Particles;* Cambridge University Press, Cambridge, UK, 2007. pp. 268–273.
33. Zammit, M.C.; Fursa, D.V.; Bray, I. Convergent-close-coupling calculations for excitation and ionization processes of electron-hydrogen collisions in Debye plasmas. *Phys. Rev. A* **2010**, *82*, 052705:1–052705:7.
34. Zammit, M.C.; Fursa, D.V.; Bray, I.; Janev, R.K. Electron-helium scattering in Debye plasmas. *Phys. Rev. E* **2011**, *84*, 052705:1–052705:15.
35. Bray, I.; Fursa, D.V. Benchmark cross sections for electron-impact total single ionization of helium. *J. Phys. B Atom. Mol. Opt. Phys.* **2011**, *44* 6, 061001:1–061001:3.
36. Griaznov V.K. *Thermophysical Properties of the Working Gas of the Gas-Phase Nuclear Reactors*; Atomizdat: Moscow, Russia, 1980.
37. Kudrin, L.P. *Statistical Plasma Physics*; Atomizdat: Moscow, Russia, 1974.
38. Ecker, G.; Müller K.G. Plasmapolarisation und Trägerwechselwirkung. *Z. Phys.* **1958**, *153*, 317–330.
39. Iglesias, C.A.; Hooper, C.F. Quantum corrections to the low-frequency-component microfield distributions. *Phys. Rev. A* **1982**, *25*, 1049–1059.
40. Iglesias, C.A. Integral-equation method for electric microfield distribution. *Phys. Rev. A* **1983**, *27*, 2705–2709.
41. Ramazanov, T.S.; Dzhumagulova, K.N. Effective screened potentials of strongly coupled semiclassical plasma. *Phys. Plasmas* **2002**, *9*, 3758–3761.
42. Anderson, P.W. Pressure broadening in the microwave and infra-red regions. *Phys. Rev.* **1949**, *76*, 647–661.
43. Gigosos, M.A.; González, M.A.; Cardeñoso, V. Computersimulated Balmer-alpha, -beta and -gamma Stark line profiles for non-equilibrium plasmas diagnostics. *Spectrochim. Acta Part B* **2003**, *58*, 1489–1504.
44. Seidel, J.; Stamm, R. Effects of radiator motion on plasma-broadened hydrogen Lyman-β. *J. Quant. Spectrosc. Radiat. Transfer* **1982**, *27*, 499–503.
45. González, M.A.; Gigosos M.A. Analysis of Stark line profiles for non-equilibrium plasma diagnosis. *Plasma Sourc. Sci. Technol.* **2009**, *18(3)*, 034001:1–034001:5.
46. Bruggeman, P.; Schram, D.; González, M.A.; Rego, R.; Kong, M.G.; Leys, C. Characterization of a direct dc-excited discharge in water by optical emission spectroscopy. *Plasma Sourc. Sci. Technol.* **2009**, *18(2)*, 025017:1–025017:13.

47. Xiong, Q.; Nikiforov; A.Y.; González, M.A.; Leys, C.; Lu, X.P. Characterization of an atmospheric helium plasma jet by relative and absolute optical emission spectroscopy. *Plasma Sourc. Sci. Technol.* **2013**, *22(1)*, 015011:1–025017:13.
48. Dufour, E.; Calisti, A.; Talin, B.; Gigosos, A.M.; González, M.A.; Dufty, J.W. Charge correlation effects in electron broadening of ion emitters in hot and dense plasmas. *J. Quant. Spectros. Radiat. Transf.* **2003**, *81*, 125–132.
49. Dufour, E.; Calisti, A.; Talin, B., Gigosos, M.A.; González, M.A.; del Rio Gaztelurrutia, T.; Dufty, J.W. Charge-charge coupling effects on dipole emitter relaxation within a classical electron-ion plasma description. *Phys. Rev. E* **2005**, *71*, 066409:1–066409:9.
50. Konjević, N.; Ivković, M.; Jovićević, S. Spectroscopic diagnostics of laser-induced plasmas. *Spectrochim. Acta Part B: Atom. Spectrosc.* **2010**, *65*, 593–602.
51. Hooper, C.F., Jr. Low-frequency component electric microfield distributions in plasmas. *Phys. Rev.* **1968**, *165*, 215–222.
52. Potekhin, A.Y.; Chabrier, G.; Gilles, D. Electric microfield distributions in electron-ion plasmas. *Phys. Rev. E* **2002**, *65*, 036412:1–036412:12.
53. Omar, B.; Wierling, A.; Günter, S.; Röpke, G. Analysing brilliance spectra of a laser-induced carbon Plasma. *J. Phys. A: Math. Gen.* **2006**, *39*, 4731–4737.
54. Pérez, C; Santamarta, R.; de la Rosa, M.I.; Mar, S. Stark broadening of neutral helium lines and spectroscopic diagnostics of pulsed helium plasma. *Eur. Phys. J. D* **2003**, *27*, 73–75.
55. Kelleher, D.E. Stark broadening of visible neutral helium lines in a plasma. *J. Quantit. Spectrosc. Radiat. Transf.* **1981**, *25*, 191–220.
56. Gao, H.M.; Ma, S.L.; Xu, C.M.; Wu, L. Measurements of electron density and Stark width of neutral helium lines in a helium arc plasma. *Eur. Phys. J. D* **2008**, *47*, 191–196.
57. Kobilarov, R.; Konjević, N.; Popović, M.V. Influence of ion dynamics on the width and shift of isolated He I lines in plasmas. *Phys. Rev. A* **1989**, *40*, 3871–3879.
58. Morris, R.N.; Cooper, J. Stark Shifts of He I 3889, He I 4713, and He I 5016. *Can. J. Phys.* **1973**, *51*, 1746–1751.
59. Berg, H.F.; Ali, A.W.; Lincke, R.; Griem, H.R. Measurement of stark profiles of neutral and ionized helium and hydrogen lines from shock-heated plasmas in electromagnetic T tubes. *Phys. Rev.* **1962**, *125*, 199–206.
60. Milosavljević, V.; Djeniže, S. Ion contribution to the astrophysical important 388.86, 471.32 and 501.56 nm He I spectral lines broadening. *New Astron.* **2002**, *7*, 543–551.
61. Soltwisch, H.; Kusch, H.J. Experimental Stark profile Determination of some Plasma Broadened He I- and He II Lines. *Z. Naturforsch. A* **1979**, *34a*, 300–309.
62. Omar, B.; Wierling, A.; Reinholz, H.; Röpke, G. Diagnostic of laser induced Li II plasma. *Phys. Rev. Res. Int.* **2013**, *3*, 218–227.
63. Röpke, G.; Seifert, T.; Kilimann, K. A Green's function approach to the shift of spectral lines in dense. *Ann. Phys. (Leipzig)* **1981**, *38*, 381–460.
64. Kobzev, G.A.; Iakubov, I.T.; Popovich, M.M. *Transport and Optical Properties of Nonideal Plasmas*; Plenum Press: New York, NY, USA & London, UK, 1995.

65. Redmer, R. Physical properties of dense, low-temperature plasmas. *Phys. Rep.* **1997**, *282*, 35–157.
66. Günter, S. Stark shift and broadening of hydrogen spectral lines. *Contrib. Plasma Phys.* **1989**, *29*, 479–487.
67. Kadanoff L.P.; Baym, G. *Quantum Statistical Mechanics: Green's Function Methods in Equilibrium and Nonequilibrium Problems*; Addison-Wesley Publishing Co., Inc.: New York, NY, USA, 1989.
68. Zimmermann, R. *Many Particle Theory of Highly Excited Semiconductors*; BSB Teubner: Leipzig, Germany, 1987.
69. Zimmermann, R.; Kilimann, K.; Kraeft, W.-D.; Kremp D.; Röpke, G. Dynamical screening and self energy of excitons in the electron-hole plasma. *Phys. Stat. Sol. (B)* **1978**, *90*, 175–187.
70. Omar, B. Spectral line broadening in dense plasmas. *J. Atom. Mol. Opt. Phys.* **2011**, *2011*, 850807:1–850807:8.
71. Edmonds, A.R. *Angular Momentum in Quantum Mechanics*; Princeton University Press: Princeton, NJ, USA, 1960.